Journal of the Serbian Society for Computational Mechanics / Vol. 19 / No. 1, 2025 / pp 437-450 / review paper
(10.24874/jsscm.2025.19.01.28)

COMPUTATIONAL MODELING AND PARAMETRIC STUDY OF CIRCULATING TUMOR CELL (CTC) MOTION AND ATTACHMENT IN CAPILLARIES WITH PLATELET INTERACTION AND ACTIVATION

Vladimir Simic[1] [0000-0001-7842-8902], **Miljan Milosevic**[1,2,4] [0000-0003-3789-2404], **Aleksandar Nikolic**[1] [0000-0002-7052-7444], **Shao Ning**[3] [0000-0003-2625-4546], **Xuewu Liu**[3] [0000-0002-8702-0295], **Fransisca Leonard**[3] [0000-0003-1888-6279], **Milos Kojic**[1,2,3,5*] [0000-0003-2199-5847]

[1] Institute for Information Technologies, University of Kragujevac, Kragujevac, Serbia
e-mail: **vsimic@kg.ac.rs**, **dziga@kg.ac.rs**
[2] Bioengineering Research and Development Center, Kragujevac, Serbia
e-mail: **mkojic42@gmail.com**
[3] Houston Methodist Research Institute, The Department of Nanomedicine, Houston, USA
e-mail: **nshao@houstonmethodist.org**, **xliu@houstonmethodist.org**, **fleonard@houstonmethodist.org**
[4] Belgrade Metropolitan University, Belgrade, Serbia
[5] Serbian Academy of Sciences and Arts, Belgrade, Serbia
e-mail: **mkojic42@gmail.com**
**corresponding author*

Abstract

Metastasis involves the dissemination of circulating tumor cells (CTCs) from the primary tumor, their survival in the bloodstream, and eventual colonization of distant organs. Adhesive interactions with platelets, leukocytes, and endothelial cells are critical to CTC survival and extravasation. Platelet adhesion enhances CTC viability and promotes metastasis. To investigate the biomechanical conditions governing CTC arrest, we developed a computational platform within the PAK software, integrating 2D axisymmetric solid-fluid models. This framework evaluates CTC transit through capillaries under physiological conditions and examines how capillary pressure gradients, CTC size and stiffness, and platelet size influence arrest dynamics. A parametric analysis was conducted to assess the effects of platelet number, CTC mechanical properties, and ligand-receptor bond stiffness on CTC trajectory, axial positioning, and endothelial adhesion. Both resting and thrombin-activated platelets were modeled, incorporating experimental adhesion force data via 1D finite element truss elements to simulate ligand-receptor interactions. The study establishes quantitative relationships between cellular and molecular parameters and the mechanical thresholds for CTC arrest, providing insights into early metastatic events and improving predictive models of metastasis progression. This paper is a summary of our previous publications as a document of our research related to 50 years of the development of our PAK finite element software

Keywords: metastasis process, CTCs, adhesive forces, ligand-receptor bonds, platelets

1. Introduction

Metastasis, the foremost cause of death among cancer patients, occurs when circulating tumor cells (CTCs) detach from the primary tumor, travel through the bloodstream or lymphatic system, and establish secondary tumors in distant organs. Evidence further implies that cancer cells can detach from their site of origin tumor and enter the blood or lymphatic vessels as single circulating tumor cells (CTCs) or CTC clusters is significantly influenced by intrinsic and/or extrinsic events in the microcirculation (Varotsos Vrynas et al., 2021). During circulation, CTCs encounter significant mechanical and immunological challenges, including high shear stress and immune surveillance, which eliminate most of them. However, those that survive do so by forming stable interactions with the vascular endothelium, a process that precedes extravasation and metastatic colonization. There is a high probability that most of the CTCs will be destroyed due to physical conditions that occur in blood flow, like high endothelial shear stress (Anvari et al., 2021), or due to an immune response of the body (Wirtz et al., 2011). CTCs can persist in the bloodstream and initiate metastasis only if they establish a firm interaction with the vascular wall, which represents a critical step preceding extravasation. (Chambers et al., 2002). Some of the preliminary research has shown that, in addition to size-dependent arrest in capillaries (Lucotti and Muschel, 2020), CTCs can also adhere to pre-capillary arterioles and portal venules through receptor–ligand interactions (Coman and De Long, 1951).

Although the mechanisms by which platelets act are poorly understood, there is evidence that primary tumor cells express thrombin to promote metastasis through platelets. Thrombin enhances tumor cell-induced platelet aggregation (TCIPA) in vitro by fully activating specific membrane receptors on platelets (Nierodzik et al., 1991). Recently, the role of platelets in the progression of malignant tumors has gained attention (Boucharaba et al., 2004), such as activated platelets, which are a primary source of lysophosphatidic acid (LPA), a simple lipid with growth factor-like signaling properties (Gerrard and Robinson, 1989). Moreover, recent studies showed that mechanical changes in cancer cells, such as the dynamic regulation of cell stiffness and contractility, are common phenotypic events in cancer development, progression and metastasis (Xu et al., 2012).

Despite recent advances, the precise mechanisms governing platelet-CTC interactions remain insufficiently understood. Direct experimental observations of these interactions are currently limited, necessitating computational approaches to bridge this knowledge gap. This study employs a computational model to simulate the movement of CTCs through microvessels, incorporating platelet adhesion and receptor-ligand interactions. Using a strong coupling approach and remeshing techniques, we investigate how geometric and material parameters—such as CTC size, stiffness, and platelet binding—affect metastatic potential. Additionally, microfluidic experiments validate our model by mimicking blood vessel dynamics and platelet-CTC interactions observed in vivo.

Furthermore, authors have developed and integrated a 1D finite element (rope) element to constitute active ligand-receptor bonds, enabling a detailed assessment of CTC deformation and passage through various microvessel types in the presence of platelets. The objective of the study is to provide deeper insight into the core mechanisms of metastasis, emphasizing receptor–ligand interactions involving CTCs and platelets interaction. To validate the model, we have tried to find the analogy of the computational results with experimental data obtained from a microfluidic device, that replicates different blood vessel sizes and platelet-CTC interactions in both high- and low-metastatic potential scenarios observed in vivo. This work further applies a 2D computational framework to examine CTC motion within the plasma flow,

performing a parametric analysis of critical factors and parameters, including the number of adherent platelets, CTC size and mechanical properties, and ligand–receptor bond stiffness.

2. Methodology

The primary tools utilized for this study include the Finite Element Analysis (FEA) software PAK (Kojic et al., 2010) (an abbreviation in Serbian for Program za Analizu Konstrukcija), along with CADFiS, an interactive three-dimensional graphical interface for modeling and visualization. The computational model integrated within PAK establishes a direct solid- fluid interaction using the strong coupling approach to analyze fluid flow and solid deformations.

To solve the fluid field, the Navier-Stokes equations are required in the following manner

$$\rho_f\left(\frac{\partial v_i}{\partial t}+\frac{\partial v_i}{\partial x_k}v_k\right)=-\frac{\partial p}{\partial x_i}+\mu\frac{\partial^2 v_i}{\partial x_k\partial x_k}+f_i^V \quad i=1,2,3;\quad \text{sum on } k:\ k=1,2,3 \tag{1}$$

where v_i and p represent the velocities and pressure, respectively, density is denoted as ρ_f the dynamic viscosity of the fluid presented as μ, and f_i^V in the equation correspond to volumetric forces. There is a incompressibility consideration for fluid, wherefore the following continuity equation relates

$$\frac{\partial v_i}{\partial x_i}\equiv\frac{\partial v_x}{\partial x}+\frac{\partial v_y}{\partial y}+\frac{\partial v_z}{\partial z}=0 \tag{2}$$

Equations above (1 and 2) can possibly be transformed into a weak form, applied to one finite element, using the incremental-iterative calculation scheme (Galerkin method (Kojic et al., 2008)):

$$\begin{bmatrix}\frac{1}{\Delta t}\mathrm{M}+{}^{(i-1)}_{vv} & \mathrm{K}_{vp}\\ \mathrm{K}_{vp}^T & 0\end{bmatrix}\begin{Bmatrix}\Delta\mathrm{V}^{(i)}\\ \Delta\mathrm{P}^{(i)}\end{Bmatrix}=$$
$$\begin{Bmatrix}{}^{n+1}F^{ext(i-1)}\\ 0\end{Bmatrix}-\begin{bmatrix}\frac{1}{t}\mathrm{M}+{}^{(i-1)}_{vv} & \mathrm{K}_{vp}\\ \mathrm{K}_{vp}^T & 0\end{bmatrix}\begin{Bmatrix}{}^{n+1}\Delta\mathrm{V}^{(i-1)}\\ {}^{n+1}\Delta\mathrm{P}^{(i-1)}\end{Bmatrix}+\begin{Bmatrix}\frac{1}{\Delta t}\mathrm{M}^n\mathrm{V}\\ 0\end{Bmatrix} \tag{3}$$
$$with\left[{}^{n+1}\left({}^{(i-1)}_{vv}\right)_{KJ}\right]_{ik}=\left[{}^{n+1}K_{KJ}^{(i-1)}\right]_{ii}+\left[{}^{n+1}J_{KJ}^{(i-1)}\right]_{ik}$$
$$\left[{}^{n+1}J_{KJ}^{(i-1)}\right]_{ik}=\rho\int_V N_K\,{}^{n+1}v_{i,k}^{(i-1)}N_J\,dV$$

The nodal velocity and pressure vectors (equation 3) are denoted as ***V*** and ***P*** respectively, while the ρ stands for the fluid density, n is the time step of size Δt, i is the current iteration, and the required matrices are given in (Kojic et al., 2008).

For the solid domain, a mixed formulation is employed, which is well-suited for modeling incompressible bodies immersed in incompressible fluids (Kojic, 2013). Within this framework, the stress tensor σ_{ij} is decomposed into deviatoric and volumetric components, which are subsequently incorporated into the linear momentum balance equation

$$\rho_s \frac{\partial v_i}{\partial t} = \frac{\partial \sigma'_{ik}}{\partial x_k} + \frac{\partial p}{\partial x_i} + f_i^V \quad i = 1,2,3; \quad \text{sum on } k: \; k = 1,2,3 \tag{4}$$

σ'_{ij} and p correspond to deviatoric and mean stress, respectively. The density of solid is denoted as ρ_s, while f_i^V are volumetric forces. The total strain can be decomposed into two components: deviatoric (e'_{ij}) and the volumetric (e_v), following the deviatoric strain equation (Kronecker delta symbol is given as δ_{ij}):

$$e'_{ij} = e_{ij} - \delta_{ij} e_v / 3 \tag{5}$$

after which the deviatoric stress is calculated as:

$$\sigma'_{ij} = 2Ge'_{ij} \tag{6}$$

where ***G*** is the shear modulus. The solid is treated as viscoelastic, requiring the inclusion of an additional linear relation to account for viscoelastic stresses σ_{ij}^{vE} as (D presents the damping coefficient):

$$\sigma_{ij}^{vE} = D \frac{\partial e_{ij}}{\partial t} \tag{7}$$

Subsequently, the total nodal stress sums up the linear (σ_{ij}) and the viscoelastic stress (σ_{ij}^{vE}).

The finite element (FE) balance equations governing the solid domain adopt the same formulation as those applied to the fluid (3). In this study, mixed finite elements are utilized, following the approach described by (Kojic, 2013), which enables simultaneous interpolation and solution of both displacements and stresses. Within each finite element, pressure is treated as a constant, while mean stress is interpolated analogously to the procedure used in fluid domains so that the pressure-velocity matrix $\mathbf{K}_{vp}$ has the following form

$$\mathbf{K}_{vp} = \int_V \mathbf{B}_L^T \mathbf{T}^{vT} dV \tag{8}$$

where the matrix $\mathbf{T}^v$ is

$$\mathbf{T} = \begin{bmatrix} \mathbf{T}^{vn} & \mathbf{0}^T \end{bmatrix}, \mathbf{T}^{vn} = \begin{bmatrix} 1 & 1 & 1 \end{bmatrix} \tag{9}$$

The remeshing approach serves as a basis for the solid-fluid interaction usage. In this method, as outlined in (Kojic, 2013), it is assumed that the solid-fluid interface shares common nodes with identical velocities within a given time step. Then, we solve the system of equations (3) to discover the velocity increments, under the assumption that, at the beginning of the time step, the initial velocities of the common solid and fluid nodes are equal. After the determination of the velocity increments, the displacements of the solid nodes during equilibrium iterations are obtained using the following equation:

$$\mathbf{U}^{(i)} = \mathbf{U}^t + \Delta t \mathbf{V}_s^{(i-1)} + \Delta t \Delta \mathbf{V}_s^{(i)} = \mathbf{U}^{(i-1)} + \Delta t \Delta \mathbf{V}_s^{(i)} \tag{10}$$

the index *i* next to the displacement vector $\mathbf{U}$ represents the vector of velocity (given for the current iteration), as well as the *t* stands for the velocity at the beginning of the time step.

To model contact interactions between the CTC, the capillary wall, and platelets, one-dimensional truss contact elements are employed, following the approach described by (Isailovic, 2012). The interaction is represented through repulsive stress or forces applied to solid nodes located at distances from the wall or platelet smaller than a prescribed threshold l_0. Then a force F_n normal to the surface of the cell is formed by using the equation $F_n = k(l_0 - l)$, where k is the stiffness of the fictitious spring.

Ligand–receptor forces arise from platelet activation kinetics and account for bonds established through CTC–platelet interactions. In the computational framework, these interactions are modeled using the simplified concept of active ropes (Fig. 1). An active rope is generated between a nod that belongs to the CTC (N^t) and corresponding point P (that is integral part of the wall) once their distance is below the prescribed threshold d_{min} (Fig. 1a), following the initial length of the active rope denoted as L_0. Furthermore, at the time t+dt, due to the cell movement, aforementioned point N from Fig. 1a moves to the N^{t+dt}, resulting the change of the current distance between the cell node and the wall point to L. An attractive force at a cell rope is generated at node N- $F_{LR} = k_{LR}(L - L_0)$, where the F_{LR} presents the ligand receptor force formed along the NP distance line, while k_{LR} is the stiffness of the ligand-receptor bond.

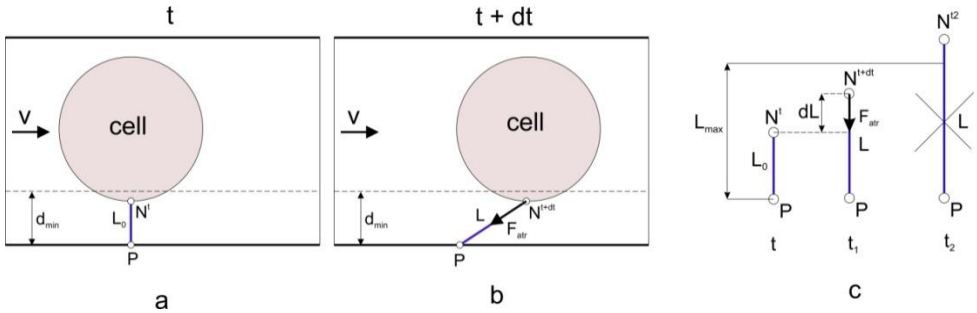

Fig. 1. Schematic representation of the active rope concept for ligand–receptor interactions: (a) cell at time t with a generated 1D active rope element of initial length L_0, b) cell at the current time $t+dt$ in case when the active rope has the current length- L, c) Illustration of the initial configuration and a subsequent state during contact. (According to (Milosevic et al., 2023)).

Ligand–receptor interactions are modeled using an elastic rope analogy, where spring-like forces are generated only under tensile loading. The stiffness of the rope reflects the cumulative effect of multiple bonds formed in close proximity, with adhesion occurring when the distance between interacting surfaces (e.g., cell–platelet, platelet–wall, or cell–wall) is less than the critical threshold L_{max}. Beyond this threshold, the ligand–receptor bond ruptures. To capture biological variability, adhesion forces are strengthened in the case of activated platelets. In parallel, solid–solid contact interactions—such as between cells, platelets, and the capillary wall—are regulated by repulsive forces applied to solid nodes within a prescribed repulsive range, thereby preventing penetration of one solid domain into another and ensuring realistic separation during interaction.

The complete computational concept and corresponding equations related to description of the platelet-cell adhesion forces correction, according to experimental results, are given in (Simic et al., 2025).

3. Finite Element Model generation and development of software architecture

The computational modeling framework, employed in this study, is based on a structured finite element (FE) simulation workflow, consisting of pre-processing, execution of the simulations, and post-processing. Model generation and preparation are performed using the in-house CAD FiS (Fields and Solids) software (Milosevic, 2020), which enables the definition of geometry, material properties for solid, boundary conditions, and flow characteristics for fluid domains. This environment also provides interfaces for configuring independent components of the system, such as capillary channels, circulating tumor cells (CTCs), and platelets, ensuring flexibility in model development. Once defined, the model is exported in a standard input format (.dat) and solved using the FE solver PAK. The solver produces numerical results that describe the evolution of key physical fields, including displacement, velocity, and pressure distributions. These outputs are stored in widely compatible file formats (.unv and .vtk), facilitating seamless integration with both the native CAD FiS post-processing environment and external visualization platforms such as Paraview. Post-processing capabilities include scalar and vector field visualization, cutting-plane views, and nodal data analysis, enabling detailed examination of stresses, velocities, and fluid–structure interactions. This workflow, illustrated in Figure 2, provides a systematic and adaptable approach for simulating complex biophysical processes. By integrating pre-processing, simulation, and post-processing into a coherent pipeline, the framework ensures both accuracy and efficiency in capturing the dynamics of CTC–platelet–wall interactions under physiological flow conditions.

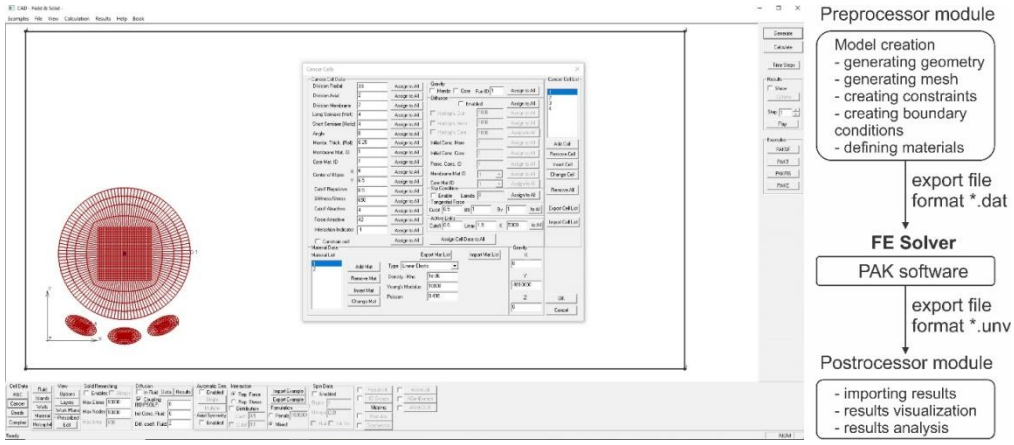

Fig. 2. User interface enviroment of CAD Field and Solid graphical pre- and post-processing software (dialog for CTC and platelet generation displayed) and Data Flow (right panel) for input/output data in pre- and post-processing software (According to (Milosevic et al., 2023)).

4. Numerical examples

A simple 2D model of capillary branching, with the deformable solid CTC entering the branching part, is shown in Fig. 3; specifically, lower branch (L_4 on Fig. 3) contains elliptical solid platelet (capillary wall attached) that narrows the channel diameter.

The model captures a simplified representation of a vascular bifurcation to study CTC dynamics under fluid flow. A circulating tumor cell (CTC), initially undeformed at the inlet channel, is transported through the main vessel segment, where it deforms under hydrodynamic forces. As it progresses into a narrower branch containing an adhered platelet, the reduced vessel diameter

induces further deformation, ultimately bringing the CTC into contact with the platelet and the vessel wall. This configuration enables investigation of CTC deformation, platelet-mediated obstruction, and cell–wall interactions within a geometrically constrained microvascular environment..

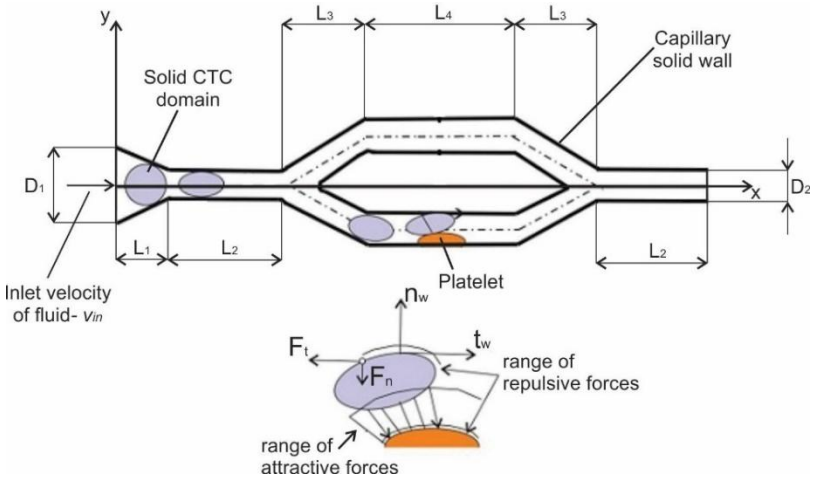

Fig. 3. Schematic representation of a circulating tumor cell (CTC) within a capillary bifurcation, where the cell diameter exceeds that of the L_2 segment, and an adhered platelet acts as an obstacle. The model geometry is characterized by defined structural parameters and prescribed inlet velocity. (According to (Milosevic et al., 2023)).

The influence of five parameters is tracked and examined, to analyze the effects of the duration contact between the CTC and the platelet: CTC diameter, platelet thickness, CTC stiffness, platelet stiffness, and ligand-receptor bond strength. Geometrical and material data, as well as the boundary conditions which are considered are the same as in (Milosevic et al., 2023).

The computational model was implemented using a two-dimensional finite element (FE) mesh, with separate discretization for the solid (CTC) and fluid domains. Mesh adaptation was performed at each simulation step to maintain numerical stability and accuracy. Simulations generally contain 1000-time steps, though the resolution and duration of individual steps were adjusted when required to account for the sensitivity of FE calculations.

4.1 Influence of the platelet thickness, CTC diameter, and the CTC stiffness - case with rigid platelet

We investigated the effect of CTC size and platelet thickness on the contact time between the two within a microvascular bifurcation model. The CTC diameter was varied from 14 μm to 17 μm, while platelet thickness ranged from 1.5 μm to 3.0 μm. The platelet was represented as a rigid body, and ligand–receptor interactions were not considered, focusing instead on mechanical and hydrodynamic contributions. Representative velocity fields at four selected time steps are shown in Fig. 4a for the case of a CTC with a diameter of 15 μm and a Young's modulus of 24.4 kPa (Haga et al., 1998), with the platelet thickness set to 1.5 μm. Under these conditions, the highest velocity in the secondary branch occurred at t=1.7 s, coinciding with the moment when the CTC was arrested by platelet contact. The influence of cell mechanics was further analyzed by varying Young's modulus from 0.5 kPa to higher values, revealing a critical threshold at which the CTC could no longer deform sufficiently to pass the constriction. Figures 4b and 4c summarize the relationship between contact time and Young's modulus for platelet

thicknesses of 1.5 μm and 2.5 μm, illustrating how both geometric and mechanical parameters govern CTC arrest.

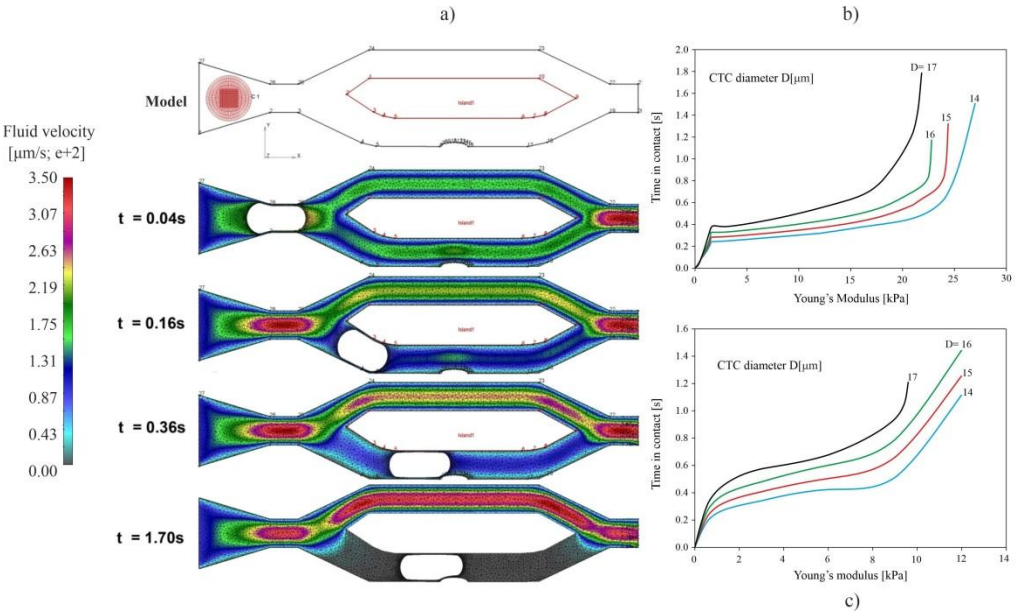

Fig. 4. a) Representation of the fluid velocity field; four random time steps displayed; from t = 0.04s - CTC entering capillary branching, up to t = 1.70s - CTC stopped in the narrowing part of the capillary. b) CTC and platelet time in contact display (Young's modulus of CTC in focus); diameters from D= 14, 15, 16, and 17 μm; Platelet thicknesses: b) 1.5, c) 2.5 μm.

4.2 Analysis of the ligand-receptor bonds influence

Here, we have examined how the presence of the ligand-receptor bonds (between platelets and CTCs) influence cell arrest. The bond stiffness (regarding the aforementioned 1D rope elements that generate attractive forces) was set at K=120 N/μm, with a force activation cutoff distance of 1 μm between the CTC and the capillary wall. The CTC diameter ranged from 14 to 17 μm, following the continual 1.5 μm space between the platelet and the capillary wall. As illustrated in Fig. 6a, ligand-receptor bonds prolong the contact time across all CTC diameters (e.g., dashed lines for D = 15 and 16 μm). Moreover, in the absence of attractive forces, the critical Young's modulus values for these diameters are higher, as shown by the continuous lines in Fig. 5a. The clear effects of ligand-receptor bond stiffness (K) are analyzed in Figs. 5b and 5c. In the first scenario (Fig. 5b), the CTC diameter varies from 14 to 17 μm, while the gap between the platelet and the wall remains fixed at 1.5 μm, along with a CTC Young's modulus of 3000 Pa. Notably, an increase in bond stiffness (K) leads to a prolonged CTC-platelet contact time. In the second scenario (Fig. 5c), the contact time is evaluated based on the cell's Young's modulus, with a constant CTC diameter of 14 μm, a 1.5 μm gap, and three different bond stiffness values. Apart from the initial segment of the curves (up to 2 kPa), where they nearly overlap, the contact time consistently increases as bond stiffness (K) rises.

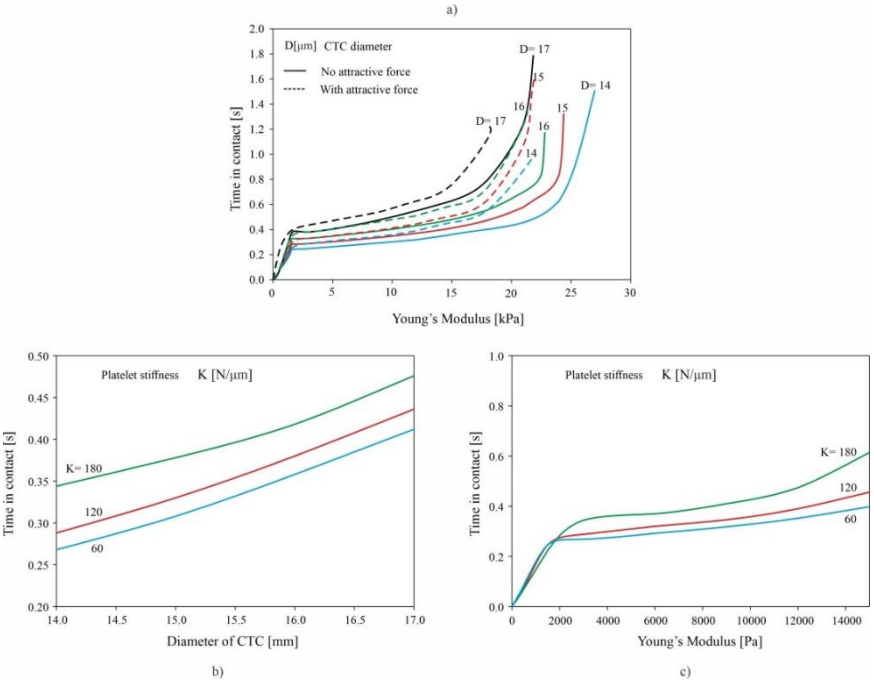

Fig. 5. (a) Contact time as a function of CTC Young's modulus, with and without attractive ligand–receptor interactions (solid lines: without attraction; dashed lines: with attraction).(b) Effect of CTC diameter on contact time for platelet thickness of 1.5 μm and ECTC=3000 Pa. (c) Effect of CTC Young's modulus on contact time for a cell diameter of 14 μm and platelet thickness of 1.5 μm.

4.3 Correlation between computational modeling and 4T1 cell perfusion with varying metastatic potential in PLT-coated gradient microfluidic chips

To mimic the architecture and hemodynamics of the hepatic microvasculature, we developed a microfluidic branching channel chip guided by morphological and flow parameters from the murine liver, including vessel diameters, lengths, and velocities. The device incorporates bifurcating channels with widths ranging from 100 μm to 12 μm, which subsequently connect to parallel arrays of 10 μm and 8 μm channels. To preserve uniform flow velocity, the number of channels at 8, 10, 12, and 15 μm was systematically adjusted, whereas for larger diameters (20–100 μm), the channel number was modulated to induce a gradual velocity increase. To suppress undesired platelet activation prior to tumor cell perfusion, channels were first blocked with BSA and subsequently coated with either intact or thrombin-activated platelets. Breast cancer 4T1 cells were then introduced via a digitally controlled syringe pump, and their arrest within the chip was monitored using an EVOS FL microscope. The fraction of 4T1 cells retained during perfusion in channels of 8–20 μm width was quantified under three conditions: without platelet coating, with non-activated platelets, and with thrombin-activated platelets, as shown in Fig. 6B.

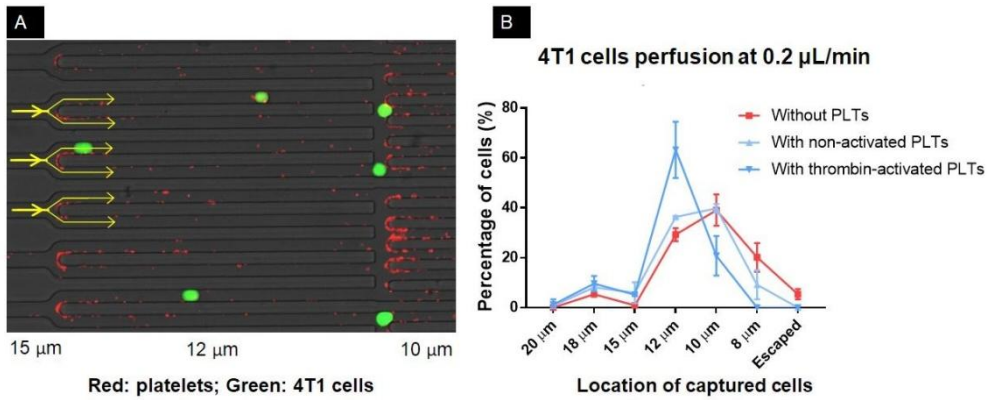

Fig. 6. Example of 4T1 Cells arrest within the Microfluidic Branching Chip. (A) Representative images of the branching microfluidic chip showing 4T1 cells (green) arrested within platelet-coated (PLT, red) channels of defined widths.(B) Percentage of 4T1 cells (mean diameter: 16 µm) retained within 8–20 µm channels during perfusion under three conditions: no PLT coating, coating with non-activated PLTs, and coating with thrombin-activated PLTs. (According to (Milosevic et al., 2023))

The number of cancer cells trapped at 10 and 12 µm channels was slightly increased but was not significant (according to results presented in Fig. 6); however, in the presence of thrombin-activated platelets, the peak retention of 4T1 cells shifted to 12 µm channels, indicating increased cell rigidity and reduced ability to traverse narrower vessels. This arrest reflects CTC accumulation at branch points where larger channels transition into smaller ones.

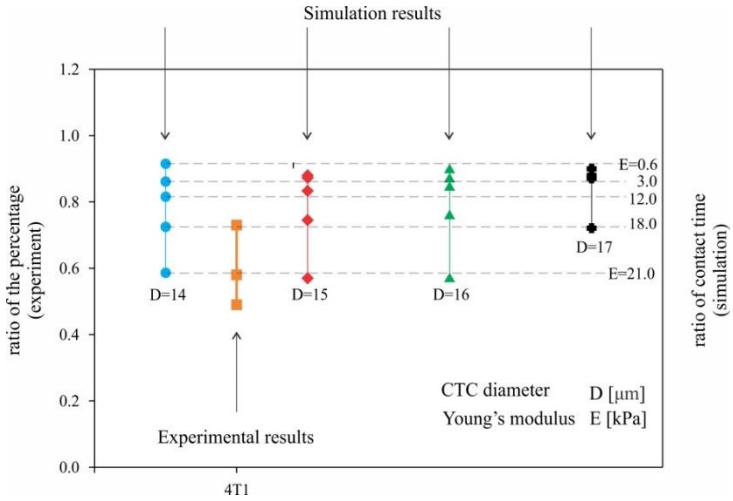

Fig. 7. Ratio of trapped cell percentage with vs. without platelet activation (experimental data; 4T1 on the x-axis) compared with the ratio of contact time with vs. without platelet activation (simulation results). Computational data are presented for four CTC diameters (D = 14–17 µm) and five stiffness values (E_{CTC} = 0.6–21 kPa). (According to (Milosevic et al., 2023)).

Correlation between experimental results and simulation, the ratio of the time in contact with/ without the attractive forces is generated (active ligand-receptor bonds) as $ratio_{sim} = (T_{non\text{-}activated}) / (T_{activated})$, ($D_{CTC}$= 14-17 μm), Young's moduli of CTC 0.6-21kPa; platelet thickness of 1.5 μm. Fig. 7 displays significant correlation between experimental and computational results.

4.4 Correlation between computational modeling and 4T1 cell perfusion with varying metastatic potential in PLT-coated gradient microfluidic chips

A 2D example of the cell motion and separate modeled platelets, within the fluid in a capillary channel, is displayed in Fig. 8. Apart from that there is no penetration between solids, adhesion forces between the cell and platelets, and between the cell and the platelets with the wall are present (schematically marked in Fig. 8a). Geometrical data, as well as the material parameters and prescribed boundary conditions (regarding the velocity in fluid), followed by the mesh quality parameters and time steps, are given in (Simic et al., 2025).

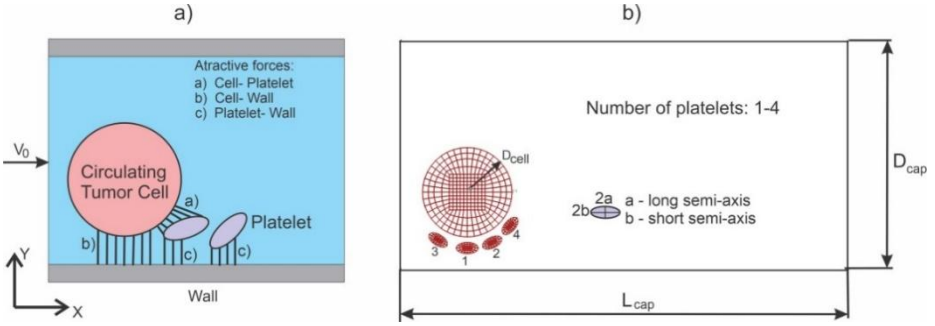

Fig. 8. Model of motion of a deformable cell within the capillary, interacting with platelets and wall. a) Schematics of adhesion forces between cell, platelets, and wall; b) Initial position of platelets with respect to cell – number of platelets is 1-4.

Our focus is to examine the influence of the number of flowing platelets for 4 diameters included, assuming the cases without platelets up to 4 platelets, for cell diameters D=8,9 [μm] (results are similar for the rest of the diameters- 10 and 11 [μm]) (solutions in Figs. 9a and 9b). Results shows that only CTC without attached platelets can reduce the ligand-receptor bond force effect and overcome the barrier of the capillary wall to flow through the channel. Hence, in case of D= 9 μm (Figs. 9b) the cell motion is limited in the case of 3 and 4 attached platelets because of fluid flow instabilities, as well as an overall increase in the number of adhesive bonds per unit surface of the cell.

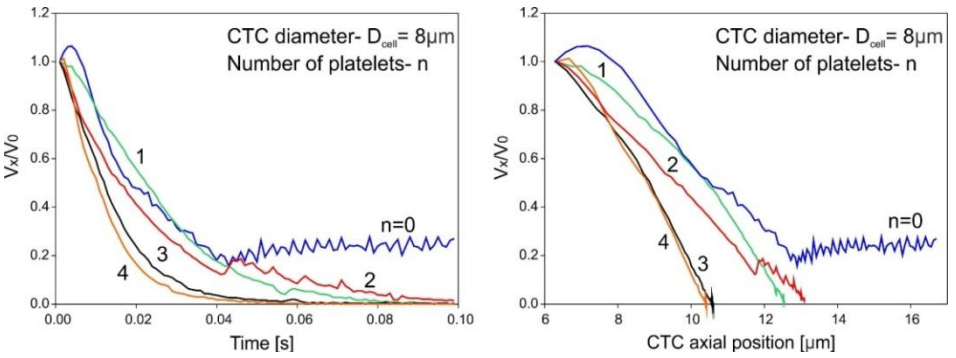

a) 8μm diameter of CTC

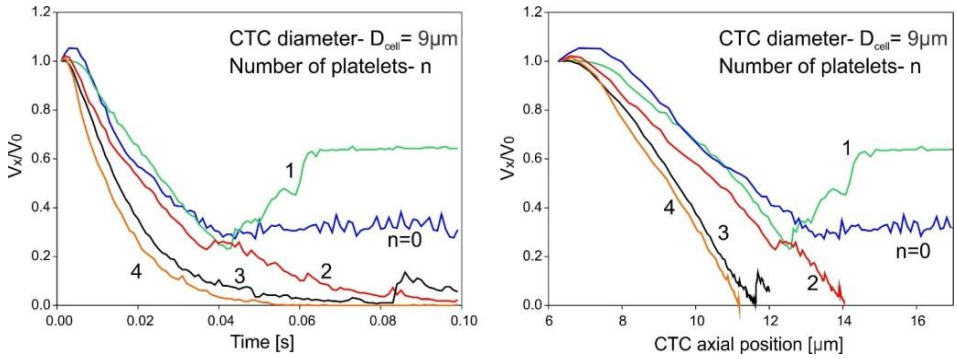

b) 9μm diameter of CTC

Fig. 9. Effects of number of platelets for 2 cell diameters. Axial Velocity–Time graphs (left) and Velocity–Axiall Position graphs (right) of the cell center, for 2 cell diameters D[μm] of CTC: a) D=8, b) D=9 (According to (Simic et al., 2025)).

5. A summary and concluding remarks

This study presents a computational model designed to investigate the behavior of circulating tumor cells (CTCs) within capillaries, particularly in the presence of platelets and adhesive interactions with the vessel wall. A key challenge in the modeling process was ensuring the CTC's passage through a stenosed capillary region and its subsequent movement through a branching network. This was achieved using virtual colliders to guide the trajectory of CTCs, enabling a more realistic simulation of their movement. The model investigates the biophysical requirements enabling large-diameter CTCs to traverse capillary stenoses and the factors governing their arrest. By analyzing factors such as CTC diameter, stiffness, fluid pressure gradient, ligand-receptor bond stiffness, and platelet thickness, the model provides insights into the mechanisms driving CTC adhesion and metastasis. A significant finding is the ability to predict how CTCs of different sizes may become arrested in the microvasculature under varying physiological conditions, particularly in relation to platelet stiffness and activation.

Platelets play a crucial role in this process. It was found that an increased number of platelets enhances CTC adhesion to the vessel wall due to alterations in the fluid flow field and a rise in overall adhesion forces. This effect is particularly pronounced for smaller-diameter CTCs, which experience stronger adhesive interactions. Additionally, softer CTCs are more prone to arrest under the same conditions, highlighting the importance of mechanical properties in metastatic progression. A key contribution of this study is the quantification of platelet activation effects using experimental data. Results indicate that activated platelets significantly enhance CTC adhesion, even in the absence of flowing platelets, underscoring their role in promoting metastasis. These findings align with increasing evidence that platelets contribute to the formation of an early metastatic niche and facilitate CTC extravasation. The computational model was validated using microfluidic experiments, demonstrating its accuracy in predicting CTC behavior. By providing a correlation between CTC physical properties and arrest dynamics, the model serves as a valuable predictive tool for understanding early metastasis. While the study utilizes a 2D framework as a simplification of real 3D conditions, it effectively captures the essential geometric and material parameters influencing metastasis.

Overall, this research offers a powerful approach to studying CTC arrest in capillaries, with implications for early cancer detection and metastasis prevention. By integrating computational

simulations with experimental data, it provides a cost-effective alternative to traditional experimental models, aiding in the development of targeted therapeutic strategies.

Acknowledgements: This work was supported by the National Institutes of Health (U01CA244107) and by the Ministry of Education, Science and Technological Development of the Republic of Serbia under contract [451-03-68/2022-14/200378, Institute of Information Technologies, University of Kragujevac]. Additional support was provided by the Center for Scientific Research of the Serbian Academy of Sciences and Arts and the University of Kragujevac [Project MODELETS], as well as by the Serbian Academy of Sciences and Arts (grant F-134). We further acknowledge the contributions of the Institute for Artificial Intelligence Research and Development of Serbia and the City of Kragujevac, Serbia.

References

Anvari S, Osei E, Maftoon N. Interactions of platelets with circulating tumor cells contribute to cancer metastasis. Sci Rep. 2021;11:–.

Boucharaba A, Serre CM, Grès S, et al. Platelet-derived lysophosphatidic acid supports the progression of osteolytic bone metastases in breast cancer. J Clin Invest. 2004;114:1714-25.

Chambers AF, Groom AC, MacDonald IC. Dissemination and growth of cancer cells in metastatic sites. Nat Rev Cancer. 2002;2:563-72.

Coman DR, De Long LR. The role of the vertebral venous system in the metastasis of cancer to the spinal column; experiments with tumor-cell suspensions in rats and rabbits. Cancer. 1951;4(3):610-8.

Gerrard JM, Robinson P. Identification of the molecular species of lysophosphatidic acid produced when platelets are stimulated by thrombin. Biochim Biophys Acta. 1989;1001:282-5.

Haga JH, Beebe T, White JG, Strony J. Quantification of the passive mechanical properties of the resting platelet. Ann Biomed Eng. 1998;26(2):268-77.

Kojic M. Simple concepts in computational mechanics – do they really work? J Serb Soc Comput Mech. 2013;7(1):1-16.

Kojic M, Filipovic N, Stojanovic B, Kojic N. Computer modeling in bioengineering: theoretical background, examples and software. Chichester (UK): John Wiley & Sons; 2008.

Kojić M, Slavković R, Živković M, Grujović N, Filipović N. PAK-FE software for structural analysis, field problems, multiphysics and biomechanics. Kragujevac: Faculty of Mechanical Engineering; 1998/2010.

Lucotti S, Musumeci A, Rossi MJ. Platelets and metastasis: new implications of an old interplay. Front Oncol. 2020;10:–.

Milosevic M, Simic V, Nikolic A, Shao N, Hashimoto C, Godin B, et al. Modeling critical interaction for metastasis between circulating tumor cells (CTCs) and platelets adhered to the capillary wall. Comput Methods Programs Biomed. 2023;107810. doi: 10.1016/j.cmpb.2023.107810.

Milosevic M. (2020). CAD Solid and Field - software for biomedical engineering research and accompanied software for the book: "Computational Models in Biomedical Engineering – Finite Element Models Based on Smeared Physical Fields: Theory, Solutions, and Software". **https://github.com/miljanmilos/CAD-Solid-Field**.

Nierodzik ML, Plotkin A, Kajumo F, et al. Thrombin stimulates tumor-platelet adhesion in vitro and metastasis in vivo. J Clin Invest. 1991;87:229-36.

Simic V, Nikolic A, Shao N, Milosevic M, Leonard F, Liu X, et al. A parametric study of motion and attachment to capillary walls of circulating tumor cells (CTCs) interacting with non-activated and activated platelets. Comput Methods Programs Biomed. 2025;264:108699. doi: 10.1016/j.cmpb.2025.108699.

Varotsos Vrynas A, Perea Paizal J, Bakal C, Au SH. Arresting metastasis within the microcirculation. Clin Exp Metastasis. 2021;38(4):337-42. doi: 10.1007/s10585-021-10109-8.

Wirtz D, Konstantopoulos K, Searson PC. The physics of cancer: the role of physical interactions and mechanical forces in metastasis. Nat Rev Cancer. 2011;11:512-22.

Xu W, Mezencev R, Kim B, Wang L, McDonald J, Sulchek T. Cell stiffness is a biomarker of the metastatic potential of ovarian cancer cells. PLoS One. 2012;7(10):e46609. doi: 10.1371/journal.pone.0046609.990-1018.